

membrane. Both profiles indicate that the membrane lipids are in the bilayer arrangement. At the same time, the average level near the center of either membrane profile is considerably higher than the level near the center of the extracted-lipids profile. This observation confirms that the bacteriorhodopsin molecules extend through the bilayer. We also find that the smallest stacking distances observed,  $\sim 50 \text{ \AA}$ , are too small to allow a good fit of calculated to observed profile diffraction. This result appears to mean that the membrane in suspension is thicker than  $50 \text{ \AA}$ ; for example, the bacteriorhodopsin molecules may project out beyond the lipid bilayer.

ALLEN E. BLAUROCK\*  
MRC Cell Biophysics Unit, Biophysics  
Department, King's College,  
London WC2B 5RL, England

GLEN I. KING†  
Cardiovascular Research Institute,  
University of California,  
San Francisco 94143

#### References and Notes

1. D. Oesterhelt and W. Stoekenius, *Proc. Natl. Acad. Sci. U.S.A.* **70**, 2853 (1973).
2. A. E. Blaurock and W. Stoekenius, *Nature (London) New Biol.* **233**, 152 (1971).
3. A. E. Blaurock, *J. Mol. Biol.* **93**, 139 (1975).
4. G. I. King, *Acta Crystallogr. Sect. A* **31**, 130 (1975).
5. D. Sayre, *Acta Crystallogr.* **5**, 843 (1952).
6. R. Henderson, *J. Mol. Biol.* **93**, 123 (1975).
7. The number of possible profiles, and these profiles themselves, can in principle be calculated as indicated in (4). However, the attempt to calculate profiles other than the one principal solution has so far been unsuccessful.
8. R. Henderson and P. N. T. Unwin, *Nature (London)* **257**, 28 (1975).
9. G.I.K. thanks J. Woodard for help with computer calculations and A.E.B. thanks A. Kernaghan for drafting figures. Both authors thank R. Henderson and N. Unwin for the personal communication that the  $\alpha$ -helices in bacteriorhodopsin fan out toward one side of the membrane. As a result, there may be room for one less lipid molecule, per bacteriorhodopsin, on the corresponding side of the membrane. Both effects will help to account for the asymmetry we have found. Supported by Public Health Service NEI special fellowship F03 EY 50, 584 (A.E.B.) and program project grant HL-06285 (G.I.K.). Contribution No. 5482 from California Institute of Technology.
- \* Present address: Division of Chemistry and Chemical Engineering, California Institute of Technology, Pasadena 91125.
- † Send reprint requests to G.I.K.

7 October 1976; revised 21 December 1976

## The Earth as a Seismic Absorption Band

**Abstract.** Attenuation of seismic waves indicates that the earth is not perfectly elastic. Dispersion accompanying absorption gives frequency-dependent "elastic" moduli, a fact that must be taken into account when inverting seismic data. Normal mode data are reinverted after correcting for absorption. The correction removes the discrepancy between body wave and free oscillation interpretations of earth structure.

The earth is often assumed to be a perfectly elastic body. One consequence of this assumption is that elastic moduli and seismic velocities do not depend on frequency. Thus, if the assumption is valid, the moduli determined from seismic body waves can be compared directly with surface wave, free oscillation, and ultrasonic laboratory results and used to compute tidal response, Chandler wobble periods, and static deformation of the lithosphere. However, "elastic" waves are nondispersive only at very high and very low frequencies, and ideal

elastic behavior is only approached at very low temperatures. The absorption of seismic body waves and the decay of free oscillations indicate that the earth is not a perfectly elastic body. It is well known that dispersion must accompany absorption (1) and therefore elastic moduli depend on frequency. The travel times of body waves and the periods of free oscillation are now known to better than 0.1 percent; the effect of dispersion over the seismic frequency band can amount to 1 percent, and it is therefore a nonnegligible effect. Jeffreys (2) has long

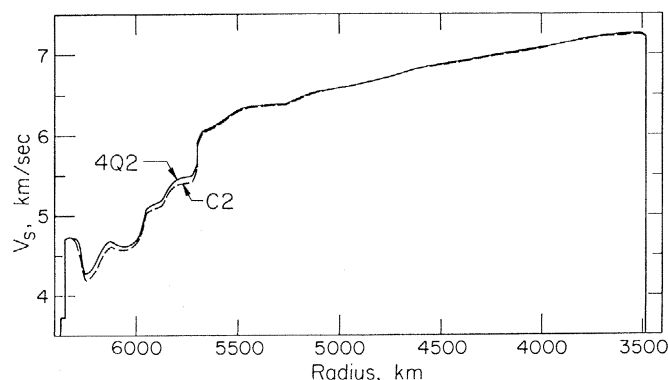


Fig. 1. Shear velocities plotted against radius for model C2, which assumes that the earth is perfectly elastic, and model 4Q2, which is based on the inversion of torsional oscillations data corrected for attenuation.

maintained that physical dispersion is important, and some attempts have been made to use the effect to reconcile body wave and surface wave earth models (3). Randall (4) recently further stressed this point. Liu *et al.* (5) calculated the dispersion-absorption for a solid having a spectrum of relaxation mechanisms, and we use their results in this report.

Relaxation phenomena are most likely to be responsible for seismic absorption (6, 7). Relaxation mechanisms include grain boundary effects, partial melting, phase changes, stress-induced atomic reordering, and thermoelasticity. Absorption in a medium with a single characteristic relaxation time,  $\tau$ , gives rise to the familiar bell-shaped Debye peak centered at a frequency  $\omega = \tau^{-1}$ . The specific dissipation function,  $Q^{-1}$ , and phase velocity satisfy the differential equation for the standard linear solid and can be written (8, 9)

$$Q^{-1}(\omega) = 2Q_m^{-1}\omega\tau/(1 + \omega^2\tau^2) \quad (1)$$

$$C^2(\omega) = C_0^2(1 + \omega^2\tau^2C_\infty^2/C_0^2)/[(1 + \omega^2\tau^2)^2 + 2\omega^2\tau^2Q_m^{-1}]^{1/2} \quad (2)$$

The high-frequency,  $C_\infty$ , and low-frequency,  $C_0$ , velocities are related by

$$\frac{C_\infty^2 - C_0^2}{C_0C_\infty} = 2Q_m^{-1}$$

In the equations above,  $Q_m^{-1}$  is the peak value of the specific dissipation function at  $\omega\tau = 1$ . The low- and high-frequency limits of  $Q^{-1}$  are, respectively,

$$Q^{-1}(\omega) = 2Q_m^{-1}\omega\tau \quad (3)$$

and

$$Q^{-1}(\omega) = 2Q_m^{-1}(\omega\tau)^{-1} \quad (4)$$

Note that the magnitude of the peak dissipation depends on the total range of velocities. The phase velocity is only constant at high and low frequencies; in these limits  $Q^{-1}$  varies as  $\omega$  or  $\omega^{-1}$ . Laboratory data on attenuation (8, 9) indicate that the absorption peak is generally much broader than given by Eq. 1. This is usually interpreted in terms of a distribution of relaxation times.

The fact that seismic values for  $Q^{-1}$  are roughly frequency-independent and are comparable in magnitude to peak attenuation values in polycrystalline oxides and silicates (10) suggests that seismic frequencies are in the midst of a broad absorption band. Shear waves reflected from the core (ScS waves) of period 10 to 50 seconds and toroidal oscillations having periods greater than 1000 seconds both sample the entire mantle and have approximately the same  $Q$  (11, 12). This suggests that  $Q$  cannot have the

strong frequency dependence implied by Eq. 3 or Eq. 4, and therefore seismic frequencies are in the midst of, rather than on the skirts of, an absorption band.

Relaxation mechanisms have been proposed for the mantle that have relaxation times spanning the seismic spectrum (6, 7). Even if a single mechanism were responsible for the absorption of seismic energy, the variations of temperature, pressure, activation energy, activation volume, grain size, dislocation length, and so forth through the mantle will serve to broaden the absorption peak. The dissipation and dispersion for a solid having a spectrum of relaxation times have been calculated by Liu *et al.* (5) and Norwick and Berry (9). The superposition of elementary relaxation peaks having a continuous distribution of relaxation times from  $\tau_1$  to  $\tau_2$  distributed as  $\tau^{-1}$  gives

$$Q^{-1} = (2Q_m^{-1}/\pi) \times \tan^{-1}[\omega(\tau_2 - \tau_1)/(1 + \omega^2\tau_1\tau_2)] \quad (5)$$

and

$$C(\omega) = C_0(1 + Q_m^{-1}/2\pi) \times \ln[(1 + \omega^2\tau_2^2)/(1 + \omega^2\tau_1^2)] \quad (6)$$

These equations were derived by Liu *et al.* (5), where a fuller discussion can be found. Liu *et al.* also gave the expression for group velocity, but this is not needed in the present discussion. An equation equivalent to Eq. 5 was derived by Savage (7) for thermoelastic attenuation in a polycrystalline solid having a distribution of grain sizes.

For  $\tau_1 \ll \omega^{-1} \ll \tau_2$  the value of  $Q$  is constant and equal to  $Q_m$ . In this frequency range the velocities at two frequencies are related by

$$C(\omega_2)/C(\omega_1) = 1 + (1/\pi Q_m) \ln(\omega_2/\omega_1) \quad (7)$$

If  $Q$  is independent of frequency in the seismic band, this equation gives the frequency-dependent correction that must be applied to surface waves and free oscillations to remove the effect of physical dispersion. This equation has also been derived from other linear theories of attenuation (1). It should be emphasized that dispersion must accompany absorption even if  $Q$  is not frequency-independent.

Velocities are higher at high frequency. If dispersion due to anelasticity is not taken into account, there will be a systematic discrepancy between body wave, surface wave, and free oscillation results, with body waves giving the higher velocities, as observed (13, 14).

The discussion so far is quite general. The relations between attenuation and

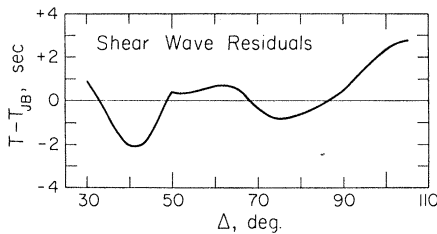


Fig. 2. Shear wave travel time residuals, relative to the Jeffreys-Bullen tables (19), as a function of distance in model 4Q2.

dispersion do not depend on a specific physical mechanism. For thermally activated grain boundary relaxation and an assumption about grain shapes in the mantle it is possible to calculate the difference between the high-frequency and low-frequency shear velocity, the relaxation time as a function of depth, and the spread of relaxation times required to satisfy the observed  $Q$  data. Using the theory of O'Connell and Budiansky (15), we calculate  $C_0/C_\infty = 0.87$  for dodecahedral grains. This gives  $\tau_1/\tau_2 \sim 10^4$  for a minimum mantle  $Q$  of 20 in shear and justifies our assumption of a broad relaxation band. In terms of temperature the relaxation time is

$$\tau = \tau_0 \exp(E^*/RT)$$

where  $\tau_0$  is the atomic jump time ( $\sim 10^{-13}$  second),  $R$  is the gas constant,  $E^*$  is the activation energy, and  $T$  is absolute temperature. The above spread in relaxation times implies a spread of about 30 kcal/mole in the activation energy of grain boundaries. For  $T = 1500^\circ\text{K}$ , the approximate temperature in the vicinity of the upper mantle low- $Q$  zone, and  $E^* = 90$  to 120 kcal/mole, relaxation times are between 1 and  $10^4$  seconds, which span the seismic band. In the lithosphere and below about 200 km the absorption band is outside the seismic band and little attenuation of seismic waves is predicted for these regions.

Surface wave phase velocities,  $C_i$ , or free oscillation periods,  $T_i$ , can be corrected to a standard period, say 1 second, by

$$\Delta C_i/C_i = -\Delta T_i/T_i = (\pi Q_i)^{-1} \ln(2\pi/\omega_i) \quad (8)$$

where  $Q_i^{-1}$  is the dissipation function for the mode having an angular frequency  $\omega_i$  (5). Thus, if  $Q$  is known for each mode in question, the correction is straightforward. However,  $Q$  is not known for many of the modes in the free oscillation data set. It can be estimated from a  $Q$  model such as MM8 (12). For toroidal oscillations the equations of Anderson *et al.* (12) give

$$-\Delta C_i/C_i = (1/\pi) \ln(\omega_i/2\pi) \times \sum_{\ell=1}^n (\partial \ln C_i / \partial \ln \beta_\ell) Q_\ell^{-1} \quad (9)$$

for a model composed of  $N$  spherical shells, where  $Q_\ell^{-1}$  is the dissipation function and  $\beta_\ell$  is the shear velocity in the layer  $\ell$ . The partial derivatives are easily calculated (16) and have been tabulated for many of the normal modes (17). A similar expression can be written for Rayleigh waves and spheroidal oscillations.

As an illustration of the effect, we take the theoretical  $Q$  model MM8 (12), correct the toroidal data (13, 14), and invert for the distribution of shear velocity and density to obtain model 4Q2. The same data set, uncorrected for anelasticity, was inverted to give model C2 (14). The two models are shown in Fig. 1. As expected, the main effect is to increase the shear velocities in the upper mantle. This removes the discrepancy between free oscillation and body wave results (13, 14) which has been attributed to large and deep differences between continental and oceanic mantle (13, 14, 18). This does not rule out lateral variations in the upper 200 km of the earth, which are well documented from both surface wave and body wave studies.

The travel time residuals for model 4Q2, compared to the shear wave travel times from the tables of Jeffreys and Bullen (19), are shown in Fig. 2. The residuals oscillate about the Jeffreys-Bullen value with an average residual of +0.4 second in the distance range  $30^\circ$  to  $105^\circ$ . This can be compared with the 4- to 5-second discrepancy between body wave and free oscillation results that results from inversion of uncorrected normal mode periods (13, 14). Thus, the effect of attenuation reconciles seismic data taken over a broad frequency band.

Model 4Q2 fits the corrected toroidal data set as well as the elastic model C2 (14) fits the uncorrected data, within 0.09 percent. A more complete inversion of the corrected normal mode data, including spheroidal modes, is in progress. Preliminary results indicate that the compressional velocity structure of the upper mantle is affected in much the same way as the shear velocity structure.

The implications of frequency-dependent elastic moduli extend beyond seismology. It is common practice to compare seismic velocities with ultrasonic data in order to infer composition. This is not valid for depths below about 100 km because of the difference in the relaxed (low-frequency, high-temperature) and unrelaxed (high-frequency, low-temperature) shear moduli. Also,

the response of the earth to deformations at tidal, annual, and Chandler periods is different from that at seismic periods. The effect of anelasticity is to make Chandler periods 1 to 2 days longer than the periods calculated for earth models constructed on the basis of short-period seismic data.

DON L. ANDERSON  
HIROO KANAMORI  
ROBERT S. HART  
HSI-PING LIU

Seismological Laboratory, California  
Institute of Technology, Pasadena 91125

#### References and Notes

1. W. Futterman, *J. Geophys. Res.* **67**, 5279 (1962); E. Strick, *Geophys. J. R. Astron. Soc.* **13**, 197 (1967); C. Lomnitz, *J. Appl. Phys.* **28**, 201 (1957); H. Kolsky, *Philos. Mag.* **8**, 693 (1956).
2. H. Jeffreys, *Nature (London)* **208**, 675 (1965).
3. E. Carpenter and D. Davies, *ibid.* **212**, 134 (1966).
4. M. Randall, *Phys. Earth Planet. Inter.* **12**, 1 (1976).
5. H. Liu, D. Anderson, H. Kanamori, *Geophys. J. R. Astron. Soc.* **47**, 41 (1976).
6. D. Anderson, *ibid.* **14**, 135 (1967); J. Vaisnys, *J. Geophys. Res.* **73**, 7675 (1968); D. Jackson, *Proc. Natl. Acad. Sci. U.S.A.* **68**, 1577 (1971).
7. J. Savage, *J. Geophys. Res.* **70**, 3935 (1965).
8. C. Zener, *Elasticity and Anelasticity of Metals* (Univ. of Chicago Press, Chicago, 1948); S. Kogan, *Izv. Acad. Sci. USSR Earth Phys.* **11**, 3 (1966).
9. A. S. Norwick and B. S. Berry, *IBM J. Res. Dev.* **5**, 297 (1961).
10. R. Gordon and C. Nelson, *Rev. Geophys.* **4**, 457 (1966); D. Jackson, *Geophys. J. R. Astron. Soc.* **25**, 25 (1971).
11. D. Anderson and R. Kovach, *Proc. Natl. Acad. Sci. U.S.A.* **51**, 168 (1964); S. Smith, *Tectonophysics* **13**, 601 (1972).
12. D. Anderson, A. Ben-Menahem, C. Archambeau, *J. Geophys. Res.* **70**, 1441 (1965).
13. T. Jordan and D. Anderson, *Geophys. J. R. Astron. Soc.* **36**, 411 (1974); F. Gilbert and A. Dziewonski, *Philos. Trans. R. Soc. London Ser. A* **278**, 187 (1975).
14. D. Anderson and R. Hart, *J. Geophys. Res.* **81**, 1461 (1976).
15. R. O'Connell and B. Budiansky, *ibid.* **79**, 5412 (1974).
16. D. Anderson, *Bull. Seismol. Soc. Am.* **54**, 681 (1964).
17. \_\_\_\_\_, *ibid.*, p. 681; \_\_\_\_\_ and R. Kovach, *ibid.* **59**, 1667 (1969); R. Wiggins, *Phys. Earth Planet. Inter.* **1**, 20 (1968).
18. T. Jordan, *Nature (London)* **257**, 745 (1975).
19. H. Jeffreys and K. Bullen, *Seismological Tables* (British Association for the Advancement of Science, London, 1940).
20. We are indebted to Sir Harold Jeffreys, who has consistently maintained that free oscillation and body wave data could not be compared directly because of the importance of damping. The role of damping has also been recognized by D. Davies, E. Carpenter, C. Lomnitz, and M. J. Randall. We wish to particularly thank M. J. Randall, who pointed out to us the inadequacy of current treatments of attenuation. This research was supported by the Advanced Research Projects Agency of the Department of Defense and was monitored by the Air Force Office of Scientific Research under contract F44620-77-C-0022. Contribution No. 2740, Division of Geological and Planetary Sciences, California Institute of Technology.

16 August 1976; revised 7 December 1976

## Nuclear Morphometry During the Cell Cycle

**Abstract.** *Directly measured and derived geometric and densitometric parameters were obtained by means of the automated image analyzer Quantimet 720-D in Feulgen-stained HeLa cells synchronized by selective mitotic detachment. These data indicate substantial alteration of nuclear morphology during the entire cell cycle, even during the G1 and G2 phases, and the late G1-early S and late S-G2 transitions.*

Recent chemical and physicochemical studies of chromatin isolated from bulk populations of synchronized cells suggest that chromatin conformation (1, 2) and levels of nuclear protein phosphorylation (3) change throughout the mammalian cell cycle, parallel to other physical-chemical and autoradiographic parameters (4). Attempts have been made to correlate these variations with the mechanisms that control cellular proliferation and S phase DNA replication (2, 3). It is, however, difficult to estimate the degree to which measurement artifacts are introduced in these determinations by the physical alterations of macromolecular structure which are produced during the process of fractionation of cell constituents. For instance, there is evidence that the structural and functional properties of native chromatin are drastically altered by shearing during the isolation procedure (5, 6). It is desirable to determine quantitative changes in chromatin during the cell cycle in situ, that is, in

cells that are morphologically intact. The DNA content of Feulgen-stained cell nuclei and chromosomes may be estimated by means of the integrated optical density (I.O.D.) obtained by scanning densitometers (7). Measurement artifacts usually arise from random processes such as variation in nuclear thickness and electrical noise in the measurement system, thus making statistical analysis necessary. These studies determined that differences in mean values of nuclear geometric parameters and I.O.D. (DNA content) exist between images obtained from cells that were synchronized and harvested at various intervals throughout the HeLa S3 cell cycle.

Several alternative approaches to texture analysis have already been used successfully in various fields of life science (8).

We measured the following parameters for each nuclear image at the base threshold [0.04 optical density (O.D.)]: I.O.D., area, projection, and perimeter.

We also computed these derived parameters from measured values—average O.D. for each nuclear image (obtained by dividing the area of the nuclear image by the square of its parameter) and mean bounded path (obtained by dividing the area of a nuclear image by its horizontal projection). In this case the horizontal projection consisted of the linear sum of all lagging edges projected against a vertical line.

We used the Quantimet 720-D automated image analyzer for these experiments, which was equipped with a plumbicon scanner and 720-D densitometer module (Cambridge Instrument) (9), and a Reichert Zetopan research microscope, equipped with an 80- $\mu\text{m}$  stage driven by a stepping motor. A 100-watt tungsten halogen light source was used, equipped with a 546-nm filter (40-nm bandwidth; Fish-Sherman). The condenser aperture was 1.35; the objective was  $100 \times$  oil immersion planar achromat with open iris and a numerical aperture of 1.25. Internal magnification was  $10 \times$ , produced by a Reichert high-quality, direct coupled magnification changer.

The area scanned by the Quantimet is comprised of 880 by 688 picture points which are subdivided into a 32 by 24 shade correction matrix. A featureless area of the specimen is imaged and loaded into the shade corrector matrix. This provides a multipoint image loading of shading with omnidirectional interpolation throughout and across matrix squares. During specimen analysis, the video signal is routed through the shade corrector that modulates the signal to provide on-line background smoothing. The shade corrector compensates for local gray level differences in the image and provides a flat background field throughout the scanned region. The linear dimension of the square picture points was determined at the magnification used by means of a stage micrometer (American Optical) graduated in 20- $\mu\text{m}$  divisions. The frame was adjusted to include leading and trailing edges at a given distance, and the frame width in picture points was read from the display (repeated ten times and averaged). The resultant mean picture point width (0.089  $\mu\text{m}$ ) was then entered into the data acquisition program and formed the basis for all measurements of length and area. Final system performance was checked by measuring the I.O.D. and area of a single nucleus (Fig. 1), which was manually positioned at seven different locations within the scanning field—one in the center of the field, one in each corner, and two on the center line (at the top